JACS
JOURNAL OF THE AMERICAN CHEMICAL SOCIETY
Article
pubs.acs.org/JACS

B_{22}^- and B_{23}^-: All-Boron Analogues of Anthracene and Phenanthrene

Alina P. Sergeeva,[†,§] Zachary A. Piazza,[‡,§] Constantin Romanescu,[‡] Wei-Li Li,[‡] Alexander I. Boldyrev,*[,†] and Lai-Sheng Wang*[,‡]

[†]Department of Chemistry and Biochemistry, Utah State University, Logan, Utah 84322, United States
[‡]Department of Chemistry, Brown University, Providence, Rhode Island 02912, United States

Supporting Information

ABSTRACT: Clusters of boron atoms exhibit intriguing size-dependent structures and chemical bonding that are different from bulk boron and may lead to new boron-based nanostructures. We report a combined photoelectron spectroscopic and ab initio study of the 22- and 23-atom boron clusters. The joint experimental and theoretical investigation shows that B_{22}^- and B_{23}^- possess quasi-planar and planar structures, respectively. The quasi-planar B_{22}^- consists of fourteen peripheral atoms and eight interior atoms in a slightly buckled triangular lattice. Chemical bonding analyses of the closed-shell B_{22}^{2-} species reveal seven delocalized π orbitals, which are similar to those in anthracene. B_{23}^- is a perfectly planar and heart-shaped cluster with a pentagonal cavity and a π-bonding pattern similar to that in phenanthrene. Thus, B_{22}^- and B_{23}^-, the largest negatively charged boron clusters that have been characterized experimentally to date, can be viewed as all-boron analogues of anthracene and phenanthrene, respectively. The current work shows not only that boron clusters are planar at very large sizes but also that they continue to yield surprises and novel chemical bonding analogous to specific polycyclic aromatic hydrocarbons.

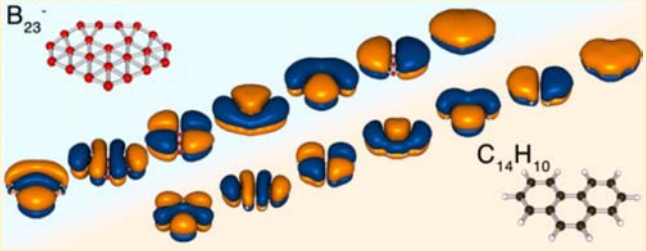

1. INTRODUCTION

Although elemental boron in the bulk is characterized by a large variety of allotropes comprised of three-dimensional (3D) cage structural units,[1] joint experimental and computational investigations over the past decade have shown that boron clusters exhibit planar or quasi-planar structures in their ground states at least to B_{21}^- in the anions,[2−14] B_{20} in the neutrals,[5] and B_{16}^+ in the cations.[15] The omnipresence of cage structures, in particular, the icosahedral B_{12} cage, among the boron allotropes and boranes, led to the hypothesis that 3D cage structures might occur for small boron clusters in early experimental studies.[16] However, subsequent computational studies suggested that icosahedral cage structures for B_{12} and B_{13} were unstable.[17] Further computational studies proposed that neutral and cationic boron clusters up to 14 atoms were more stable in the planar or quasi-planar (2D) geometries.[18] Although clusters of boron's neighbors in the periodic table had been extensively studied, experimental characterization of the structural evolution of boron clusters was not available until our photoelectron spectroscopy (PES) investigations of size-selected boron cluster anions about a decade ago.[2−4] Over the past 10 years, through joint PES and ab initio studies, we have elucidated the structural evolution of anionic boron clusters up to B_{21}^-.[2−13] Even though a double-ring 3D structure was found to be more stable at B_{20} for neutral clusters[5] and at B_{16}^+ for cationic clusters,[15] negatively charged clusters have been shown to be planar even at B_{21}^-.[13]

More importantly, our chemical bonding analyses have revealed that two-dimensional (2D) electron delocalization plays important roles in the stability of these 2D clusters, giving rise to the concepts of aromaticity, multiple aromaticity/anti-aromaticity, and analogies between boron clusters and hydrocarbons. These concepts have provided intuitive rationales for the unusual stability of boron clusters as 2D structures, which also underlie the stability of the recently proposed 2D boron sheets in analogy to graphene.[19] The following species, B_8^{2-} and B_9^-;[3,20] B_{10}, B_{11}^-, and B_{12};[4] and the B_{13}^+ cation[6,21] each have three occupied π canonical molecular orbitals and have been considered all-boron analogues of benzene, all with six delocalized π electrons satisfying the $4n + 2$ Hückel rule for π aromaticity. The unprecedented molecular wheel structures and aromaticity in B_8^{2-} and B_9^- have inspired the recent design and characterization of a series of metal-centered monocyclic boron rings, $M@B_n^-$.[22] B_{13}^- and B_{14}, each with 8 π electrons, are considered to be π anti-aromatic according to the $4n$ Hückel rule, conforming to their elongated shapes.[4] B_{16}^{2-} and B_{17}^-, each with 10 delocalized π electrons have been shown to be analogous to naphthalene ($C_{10}H_8$).[8,12]

The B_{19}^- cluster has been found to possess a highly circular spider-web-like structure with a 13-atom outer ring and an internal B-centered pentagonal unit.[10] It is doubly π aromatic, consisting unprecedentedly of two concentric π systems,

Received: August 6, 2012
Published: October 3, 2012

   dx.doi.org/10.1021/ja307605t | J. Am. Chem. Soc. 2012, 134, 18065−18073

analogous to coronene. The unique structure and bonding of B_{19}^- has inspired the proposal of a molecular Wankel motor, because the barrier of the in-plane internal rotation of the inner pentagonal system against the 13-atom peripheral ring is found to be quite low.[23] Similar fluxional behavior has also been found subsequently in the planar B_{13}^+ cluster for its internal B_3 triangle.[24] It has even been suggested recently that circularly polarized light can be used to achieve a desirable unidirectional rotation, rendering a photodriven molecular Wankel motor.[25] While all anionic planar boron clusters up to B_{20}^- consist of a peripheral boron ring bonded by localized B−B σ bonds and an inner network of atoms exhibiting delocalized σ and π bonding patterns, recently, our study of the B_{21}^- system revealed the presence of the first two-center two-electron (2c−2e) σ bond within the inner boron networks of its two lowest energy isomers.[13] It is proposed that this bonding pattern exists due to cavities within a triangular lattice framework, much like those found in the BC_3 honeycomb sheet.[26] The structures and aromaticity of the small boron clusters have been reaffirmed by recent computational studies.[27]

As the size of the cluster increases, the global minimum search becomes a daunting task and new global search methods are needed.[28] We have developed a new global minimum search method, called Cartesian walking (CW), which is designed for more efficient searches for planar structures. The CW method was first applied to B_{21}^-, as recently reported.[13] In the present article, we present a joint PES and computational study of B_{22}^- and B_{23}^-. The global minimum search for B_{22}^- is done using CW exclusively, whereas both CW and coalescence kick (CK)[29] methods are used for the global minimum search of B_{23}^-. A quasi-planar structure and a 3D double-ring structure are found to be nearly degenerate in energy for B_{22}^-, although experimentally, only the quasi-planar isomer is observed. The quasi-planar structure of B_{22}^- consists of a 14-atom periphery and 8 interior atoms and it possesses a triangular lattice without any cavity, except that the interior atoms display slight out-of-plane distortion. The π bonding pattern of B_{22}^- is found to be similar to that of anthracene. The global minimum of B_{23}^- is found to be perfectly planar with a heart-shaped structure and C_{2v} symmetry. It consists of a 15-atom periphery, 8 interior atoms, and a pentagonal cavity. The B_{23}^- "nano-heart" is highly stable because there are no competing close-lying isomers. The π bonding in the B_{23}^- nanoheart is found to be similar to that in phenanthrene.

2. EXPERIMENTAL AND COMPUTATIONAL METHODS

2.1. Photoelectron Spectroscopy. The experiment was carried out using a magnetic-bottle PES apparatus equipped with a laser vaporization cluster source, details of which can be found elsewhere.[30] Briefly, negatively charged boron clusters were produced by laser vaporization of a hot-pressed isotopically enriched ^{10}B (96%) disk target. The clusters were entrained by a He carrier gas containing 5% Ar and underwent a supersonic expansion to form a collimated and vibrationally cold cluster beam. The cluster size distribution and cooling were controlled by the time delay between the pulsed valves and the vaporization laser and the resident time of the clusters in the nozzle.[31] The anionic clusters were extracted from the cluster beam and analyzed with a time-of-flight mass spectrometer. The B_{22}^- and B_{23}^- clusters were mass-selected and decelerated before being intercepted by a detachment laser beam. Due to their relatively high binding energies, only one detachment energy was used in the current study, i.e. 6.424 eV (193 nm) from an ArF excimer laser. Photoelectrons were collected at nearly 100% efficiency by the magnetic bottle and analyzed in a 3.5 m long electron flight tube. The PES spectra were calibrated using the known spectra of Bi^- and Au^-,[32] and the energy resolution of the apparatus was $\Delta E_k/E_k$ ~2.5%, i.e. ~25 meV for 1 eV electrons.

2.2. Computational Methods. We searched for the global minimum of B_{22}^- using the CW method.[13] For B_{23}^-, both the CW and CK[29] methods were employed. The CW searches for B_{22}^- and B_{23}^- were conducted at the PBE0[33] level of theory employing the 3-21G basis set[34] and the CK search for B_{23}^- was conducted using the B3LYP hybrid density functional with the 3-21G basis set. The CW method imposes constraints on a random walking process that takes place on a grid of Cartesian coordinates to generate trial structures for further optimization. Choosing various grid characteristics and walking constraints can yield either an unbiased population of trial structures or a more directed set of trial structures, each with bond lengths that are tuned to the system at hand. For this search, trial structures were generated on a large 3D grid that imposed very little structural bias, as well as grids heavily biased toward creating planar and quasi-planar trial structures. A more detailed discussion of the CW method is given in reference 13, where it was used to search the potential energy landscape of the B_{21}^- system.

The unbiased CK method generates a random set of atomic coordinates in a large box. Coordinates are then checked for connectivity (i.e., atoms that have a nearest-neighbor within a specified distance are considered connected). If there are unconnected sets of fragments, the fragments are then submitted to a coalescence procedure until all of the fragments are connected. Once all fragments are connected, further geometrical optimization occurs. This procedure produces a population of unbiased trial structures with preoptimized geometries before quantum mechanical methods are employed. The CK method is described in detail in reference 12. For each search, all isomers below 25 kcal/mol relative to the global minimum at the 3-21G level were further optimized at the B3LYP/6-311+G*[35] and PBE0/6-311+G* levels of theory. For each isomer, vibrational frequencies were calculated and imaginary frequencies were followed to ensure that each isomer examined corresponded to a minimum on the potential energy surface. Due to the presence of competitive isomers for the global minimum of B_{22}^- at the DFT/6-311+G* level, single-point calculations were conducted at the CCSD(T)[36]/6-311+G*//PBE0/6-311+G* level of theory to more accurately assess their relative energies.

Vertical detachment energies (VDEs) of the lowest isomers were calculated at the PBE0/6-311+G(2df)//PBE0/6-311+G* and B3LYP/6-311+G(2df)//B3LYP/6-311+G* levels of theory to compare with the experimental data. In each case, the first VDE was calculated as the difference in energy between the lowest anionic state and the lowest neutral state at the geometry of the anion. For B_{22}^-, the first triplet VDE was also directly calculated as the difference in energy between the lowest anionic state and the lowest triplet neutral state at the anionic geometry. Following this, vertical excitation energies of the neutral species calculated using time dependent density functional theory (TD-DFT), namely TD-PBE0 and TD-B3LYP levels were added to the first VDEs to approximate excited state transitions.

All calculations were performed using Gaussian 09.[37] Bonding analyses were conducted using the adaptive natural density partitioning (AdNDP) method[38] at the B3LYP/3-21G//B3LYP/6-311+G* level. The detailed description of the AdNDP method can be found in reference 38. AdNDP results have been shown to be insensitive to the level of theory or basis set used.[39] The *MOLEKEL* 5.4.0.8 program[40] was used for molecular structure and canonical molecular orbital (CMO) and AdNDP bond visualization.

3. EXPERIMETAL RESULTS

The photoelectron spectra of B_{22}^- and B_{23}^- at 193 nm are shown in Figures 1 and 2, respectively. The major detachment features are labeled with letters and the measured VDEs are given in Table 1, where they are compared with theoretical calculations at the B3LYP and PBE0 levels of theory. The PBE0 VDEs for the global minimum are also plotted as vertical bars in Figures 1 and 2. Commonly, the peak marked as X represents the transition between the ground electronic states

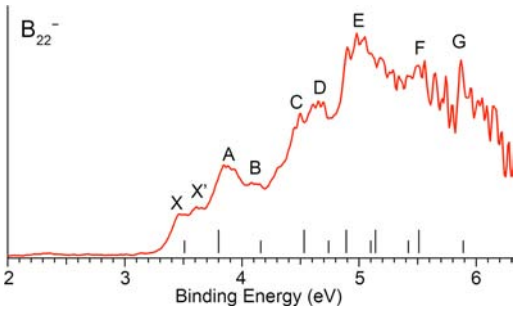

Figure 1. Photoelectron spectrum of B_{22}^- at 193 nm. Vertical bars represent calculated VDEs at the TD-PBE0/6-311+G(2df)//PBE0/6-311+G* level of theory. The short and long bars represent singlet and triplet final states, respectively. See Table 1.

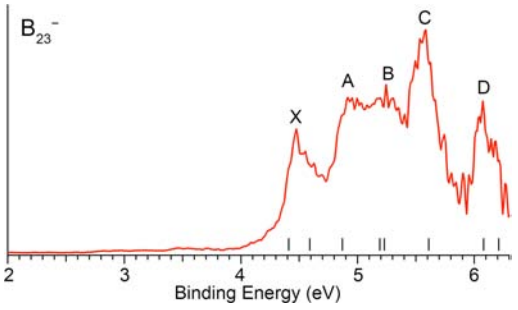

Figure 2. Photoelectron spectrum of B_{23}^- at 193 nm. Vertical bars represent calculated VDEs at the TD-PBE0/6-311+G(2df)//PBE0/6-311+G* level of theory. See Table 1.

of the anion and the neutral species, while the higher binding energy peaks (A, B,...) denote transitions to excited electronic states of the neutral cluster.

3.1. The Photoelectron Spectrum of B_{22}^-. The photoelectron spectrum of B_{22}^- (Figure 1) is quite congested with photodetachment features spanning the binding energy range from 3.3 eV to beyond 6 eV. The ground-state band X yields a VDE of 3.48 eV and an adiabatic detachment energy (ADE) of 3.34 eV. Since no vibrational structures were resolved, the ADE was estimated by drawing a straight line along the leading edge of the X band and then adding the experimental resolution to the intersection with the binding energy axis. The next resolved electronic bands are labeled as X′ (VDE: ~3.6 eV), A (VDE: 3.87 eV), and B (VDE: 4.10 eV). As will be shown below, the X′ band comes from low-lying isomers of B_{22}^-. Following a small energy gap, the spectrum displays a broader feature that is assigned to two closely spaced detachment channels, C (VDE: 4.48 eV) and D (VDE: 4.64 eV). At the high binding energy side, we observed a few more bands and tentatively assigned them as E (VDE: 5.01 eV), F (VDE: 5.51 eV), and G (VDE: 5.89 eV). The congested spectrum suggested that there might be contributions from close-lying isomers of B_{22}^-.

3.2. The Photoelectron Spectrum of B_{23}^-. In comparison to B_{22}^-, B_{23}^- has a higher binding energy and a relatively simpler spectrum (Figure 2). The first photodetachment band, X, is well resolved and seems to contain fine features due to either possible vibrational structures or overlapping detachment channels. The X band yields a VDE of 4.46 eV and an ADE of 4.32 eV. The next two features, A (VDE: 4.95 eV) and B (5.22 eV), are broad and not well resolved, indicating a possible overlap of additional detachment bands. At the high binding energy side of the spectrum, we observed a strong and well-defined resolved band C with a VDE of 5.56 eV, followed by a well-resolved band D with a VDE of 6.06 eV.

4. THEORETICAL RESULTS

4.1. The Low-Lying Structures of B_{22}^-. Searches for the global minimum and low lying isomers of B_{22}^- were done using the CW method at the PBE0/3-21G level of theory. Various grid sizes were used to direct most of the search toward planar and quasi-planar structures and also allow for the possibility of 3D isomers. Roughly 2000 trial structures were tested. A 3D tubular structure constructed manually was also considered. Due to the cost of the global searches, we refined our results for comparison with the experimental data and continued the searches for other 3D structures only if necessary. We reoptimized the lowest-lying isomers at the PBE0/6-311+G* and B3LYP/6-311+G* levels of theory, and frequencies were calculated to make sure the structures were true minima. Single-point energies were then calculated at the CCSD(T)/6-311+G*//PBE0/6-311+G* level for the four lowest-lying isomers. The results of these calculations are presented in Figure 3. The 3D tubular structure I (C_i, ^2A_u) is lowest in energy according to each level of theory. Our frequency calculation revealed that this structure has one imaginary frequency (−90 cm^{-1} at PBE0/6-311+G* level), although when this mode was followed and the structure reoptimized, the same C_i structure was returned. The next lowest in energy is the quasi-planar structure II (C_2, ^2B), only 0.78 kcal/mol higher at the CCSD(T) level (Figure 3). Structures I and II can be considered degenerate within the accuracy of our calculations. The quasi-planar structure II comprises a 14-atom peripheral ring with 8 interior atoms and can be described as a buckled triangular lattice (the maximum out-of-plane distortion is 0.93 Å). The next lowest in energy are structures III and IV, which are 1.79 and 2.44 kcal/mol higher in energy, respectively, according to the CCSD(T)/6-311+G* level of theory. These two isomers are also quasi-planar, each with 14 peripheral atoms and 8 inner atoms, except they each contain a hole in the lattice. Structures I−IV are all low enough in energy to warrant comparison with the experimental spectrum.

It should be pointed out that we encountered high norm values in the CCSD(T) calculations of the B_{22}^- isomers[41] and could not converge any of the CASSCF single-point calculations of the isomers. This suggests the multiconfigurational nature of B_{22}^- and therefore the relative energies obtained using CCSD(T) level of theory are questionable. The best we could do in this case was to compute the VDEs for all the low-lying isomers (Table 1 and Tables S1−S3) to see which structure agrees with the photoelectron spectrum of B_{22}^-. As will be discussed below, the quasi-planar (C_2, ^2B) isomer appears to be a major contributor to the photoelectron spectrum with structures III and IV being minor contributors.

4.2. The Global Minimum and Low-Lying Structures of B_{23}^-. We used both the CK and CW methods to search for the global minimum and low-lying isomers of B_{23}^-. The CK searches were performed at the B3LYP/3-21G level, while the CW searches were performed at the PBE0/3-21G level. The lowest-lying isomers were reoptimized at the PBE0/6-311+G*, and B3LYP/6-311+G* levels, and frequencies were calculated to ensure that each isomer is a true minimum. The results are presented in Figure 4. Both searches revealed a perfectly planar C_{2v} closed-shell structure V as the global minimum with no competing close-lying isomers at the PBE0/6-311+G* and B3LYP/6-311+G* levels of theory. This structure has a heart

dx.doi.org/10.1021/ja307605t | J. Am. Chem. Soc. 2012, 134, 18065−18073

Table 1. Comparison of the Experimental VDEs with the Calculated Values for B_{22}^- (C_2, ^2B) and B_{23}^- (C_{2v}, $^1A_1$); All Energies Are in eV

	VDE (exp)[a]	final state and electronic configuration	VDE (theoretical) TD-B3LYP[b]	VDE (theoretical) TD-PBE0[c]
		B_{22}^- (C_2, ^2B)		
X	3.48 (5)	^1A, {...13b^2 14a^2 14b^2 15a^2 16a^2 15b^2 16b^2 17a^2 17b^0}	3.34	3.51
A	3.87 (4)	^3B, {...13b^2 14a^2 14b^2 15a^2 16a^2 15b^2 16b^2 17a^1 17b^1}	3.73	3.80
B	4.10 (5)	^1B, {...13b^2 14a^2 14b^2 15a^2 16a^2 15b^2 16b^2 17a^1 17b^1}	4.02	4.16
C	4.48 (5)	^3A, {...13b^2 14a^2 14b^2 15a^2 16a^2 15b^2 16b^1 17a^2 17b^1}	4.36	4.53
D	4.64 (4)	^1A, {...13b^2 14a^2 14b^2 15a^2 16a^2 15b^2 16b^1 17a^2 17b^1}	4.54	4.74
E	5.01 (5)	^3A, {...13b^2 14a^2 14b^2 15a^2 16a^2 15b^1 16b^2 17a^2 17b^1}	4.82	4.89
		^1A, {...13b^2 14a^2 14b^2 15a^2 16a^2 15b^1 16b^2 17a^2 17b^1}	4.97	5.10
		^3B, {...13b^2 14a^2 14b^2 15a^2 16a^1 15b^2 16b^2 17a^2 17b^1}	5.02[d]	5.14[d]
		^1B, {...13b^2 14a^2 14b^2 15a^2 16a^1 15b^2 16b^2 17a^2 17b^1}	5.29	5.42
F	5.51 (5)	^3B, {...13b^2 14a^2 14b^2 15a^1 16a^2 15b^2 16b^2 17a^2 17b^1}	5.38	5.51
G	5.89 (4)	^1B, {...13b^2 14a^2 14b^2 15a^1 16a^2 15b^2 16b^2 17a^2 17b^1}	5.66[d]	5.89[d]
		^3A, {...13b^2 14a^2 14b^1 15a^2 16a^2 15b^2 16b^2 17a^2 17b^1}	6.17[d]	6.34[d]
		B_{23}^- (C_{2v}, $^1A_1$)		
X	4.46 (3)	$^2B_1$, {...2b$_1^2$14a$_1^2$3b$_1^2$12b$_2^2$13b$_2^2$2a$_2^2$15a$_1^2$3a$_2^2$4b$_1^1$}	4.32	4.41
		$^2A_2$, {...2b$_1^2$14a$_1^2$3b$_1^2$12b$_2^2$13b$_2^2$2a$_2^2$15a$_1^2$3a$_2^1$4b$_1^2$}	4.38	4.59
A	4.95 (4)	$^2A_1$, {...2b$_1^2$14a$_1^2$3b$_1^2$12b$_2^2$13b$_2^2$2a$_2^2$15a$_1^1$3a$_2^2$4b$_1^2$}	4.83	4.87
B	5.22 (5)	$^2A_2$, {...2b$_1^2$14a$_1^2$3b$_1^2$12b$_2^2$13b$_2^2$2a$_2^1$15a$_1^2$3a$_2^2$4b$_1^2$}	4.97	5.19
		$^2B_2$, {...2b$_1^2$14a$_1^2$3b$_1^2$12b$_2^2$13b$_2^1$2a$_2^2$15a$_1^2$3a$_2^2$4b$_1^2$}	5.04	5.23
C	5.56 (3)	$^2B_2$, {...2b$_1^2$14a$_1^2$3b$_1^2$12b$_2^1$13b$_2^2$2a$_2^2$15a$_1^2$3a$_2^2$4b$_1^2$}	5.45	5.61
D	6.06 (3)	$^2B_1$, {...2b$_1^2$14a$_1^2$3b$_1^1$12b$_2^2$13b$_2^2$2a$_2^2$15a$_1^2$3a$_2^2$4b$_1^2$}	5.90[d]	6.08[d]
		$^2A_1$, {...2b$_1^2$14a$_1^1$3b$_1^2$12b$_2^2$13b$_2^2$2a$_2^2$15a$_1^2$3a$_2^2$4b$_1^2$}	6.03	6.21
		$^2B_1$, {...2b$_1^1$14a$_1^2$3b$_1^2$12b$_2^2$13b$_2^2$2a$_2^2$15a$_1^2$3a$_2^2$4b$_1^2$}	6.56[d]	6.74[d]

[a]Numbers in parentheses represent the uncertainty in the last digit. [b]VDEs were calculated at the TD-B3LYP/6-311+G(2df)//B3LYP/6-311+G* level of theory. [c]VDEs were calculated at the TD-PBE0/6-311+G(2df)//PBE0/6-311+G* level of theory. [d]VDE corresponds to transitions of multiconfigurational nature.

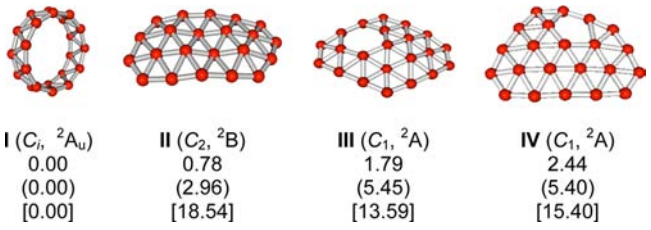

Figure 3. Low-lying isomers of B_{22}^-. Relative energies are given in kcal/mol at the CCSD(T)/6-311+G*//PBE1PBE/6-311+G*, PBE1PBE/6-311+G* (in parentheses), and B3LYP/6-311+G* (in square brackets) levels of theory. The PBE1PBE/6-311+G* and B3LYP/6-311+G* numbers have been corrected for zero-point vibrational energies at their respective levels of theory, whereas the CCSD(T) energies have been corrected for zero-point vibrational energy using the PBE1PBE/6-311+G* values. The solid rods do not necessarily represent bonding between boron atoms; B−B distances of less than 2.0 Å were connected to help visualization.

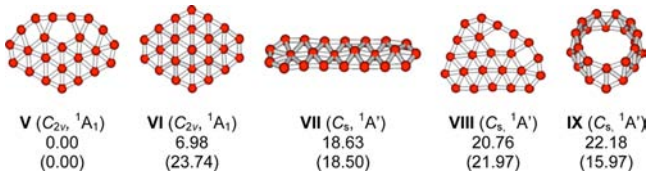

Figure 4. Global minimum and representative higher energy isomers of B_{23}^-. Relative energies are given in kcal/mol at the PBE1PBE/6-311+G* and B3LYP/6-311+G* (in parentheses) levels of theory and have been corrected for zero-point vibrational energies at their corresponding levels of theory. The solid rods do not necessarily represent bonding between boron atoms; B−B distances of less than 2.0 Å were connected to help visualization.

shape consisting of a 15-atom periphery, 8 interior atoms, and a pentagonal hole. The second low-lying isomer VI is 6.98 and 23.74 kcal/mol higher in energy at PBE0 and B3LYP levels, respectively. The isomer is quasi-planar also with C_{2v} symmetry and a buckled triangular lattice. The next isomer (structure VII) has an elongated shape and is much higher in energy, ∼19 kcal/mol relative to the global minimum at both PBE0 and B3LYP levels. Isomer VIII at 20.76 kcal/mol is a low-symmetry planar structure also with a pentagonal hole like the global minimum. Finally, the 3D double-ring-like structure IX is found to be much higher in energy, ∼22 kcal/mol higher in energy, than the global minimum at the PBE0/6-311+G* level.

The calculated VDEs for the global minimum heart-shaped B_{23}^- are compared with the experimental data in Table 1. We also calculated VDEs of the second lowest isomer VI, as shown in Table S4 (SI).

5. COMPARISON BETWEEN EXPERIMENT AND THEORY

5.1. B_{22}^-. As shown in Table S1 (SI), the double-ring tubular structure of B_{22}^- gives a very low first VDE of ∼3.1 eV, which is significantly lower than the experimental first VDE at 3.48 eV. In addition, the calculated spectral pattern including the higher VDEs does not agree with the experimental spectrum. Thus, the tubular structure can be ruled out as a contributor to the observed spectrum of B_{22}^-. This situation is

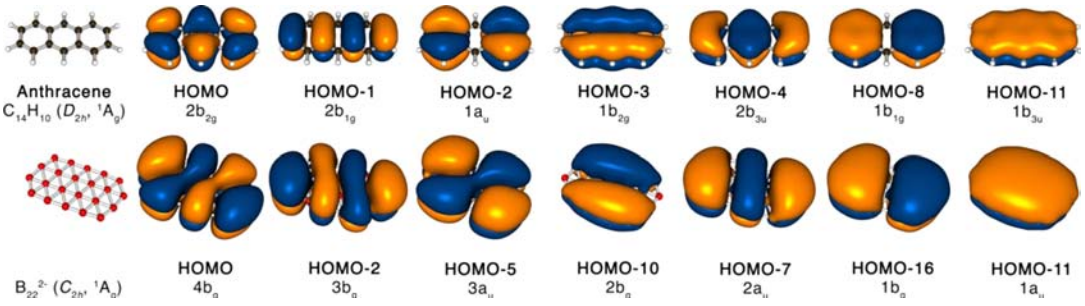

Figure 5. Comparison of the π molecular orbitals in the flattened B_{22}^{2-} cluster with those in anthracene.

similar to B_{20}^-, for which a double-ring structure was computed to be nearly degenerate with a 2D structure, but had to be ruled out as a contributor to the observed PES spectra on the basis of the calculated VDEs and comparison between experiment and theory.[5]

The calculated VDEs of the quasi-planar C_2 structure of B_{22}^- (Figure 3) agree very well with the major PES features, as shown in Figure 1 and Table 1. Table 1 compares the calculated VDEs at B3LYP and PBE0 levels with the experimental data. The two levels of theory give similar VDEs, but the PBE0 values are in slightly better agreement with experiment and will be used in the following discussion. The PBE0 values are also plotted as vertical bars in Figure 1 for easier comparison. The first calculated VDE from electron detachment of the 17b HOMO is 3.51 eV at PBE0, in excellent agreement with the experimental value of 3.48 ± 0.05 eV. The next electron detachment occurs from the 17a HOMO−1, leaving the final neutral B_{22} species in the lowest triplet state. The calculated VDE of this detachment channel is 3.80 eV, in good agreement with band A at 3.87 eV. The corresponding detachment into the singlet final state has calculated VDE of 4.16 eV, in good agreement with band B at 4.10 eV. Note that the higher intensity for band A relative to those of bands X and B is consistent with its higher spin multiplicity. The calculated VDEs for higher detachment channels from the quasi-planar C_2 structure of B_{22}^- are all in reasonable agreement with the observed experimental features, as seen in Figure 1 and Table 1.

However, the X′ feature observed at ∼3.6 eV cannot be accounted for by the C_2 isomer of B_{22}^-. Both isomers III and IV are low in energy relative to the C_2 isomer and are expected to be populated in the cluster beam. Indeed, the calculated first VDE for isomer III is 3.67 eV at B3LYP and 3.84 eV at PBE0 (Table S2 [SI]) and the calculated first VDE for isomer IV is 3.51 eV at B3LYP and 3.70 at PBE0 (Table S3 [SI]). These values are all higher than the calculated first VDE for the C_2 isomer and are in good accord with the observed X′ feature at ∼3.6 eV (Figure 1). Therefore, both isomers III and IV should be present in the cluster beam, giving rise to the observed X′ feature. In fact, the broad spectral features for B_{22}^- provide indirect evidence for the existence of multiple isomers in the cluster beam. Thus, the theoretical results are in good agreement with the experimental observations, lending credence to the identified global minimum C_2 structure for B_{22}^- and the ranking of isomers II−IV. However, the absence of the double-ring isomer I in the cluster beam deserves some comment. The absence of this isomer in the cluster beam could be due to kinetic reasons because of its major structural differences with the planar structures. This argument has been used previously to interpret the absence of the similarly low-energy double-ring isomer for B_{20}^-.[5] However, another more likely possibility concerns the actual stability of the different isomers. Due to the multiconfigurational nature of B_{22}^- as mentioned in section 4.1, even the single-point CCSD(T) energy may not be reliable. Thus, we conclude that the C_2 isomer is the one we observed in the photoelectron spectrum of B_{22}^-.

5.2. B_{23}^-. We have calculated the VDEs of the two lowest structures identified for B_{23}^- (Tables 1 and S4 (in SI). The other isomers were found to be higher in energy by 18 kcal/mol in energy (Figure 4) and they can be safely ruled out in comparison with experiment. The second lowest isomer of B_{23}^- gives a very low first VDE of 3.21 eV at B3LYP and 3.33 eV at PBE0 (Table S4) and can also be ruled out to have any contribution in comparison to the observed spectrum (Figure 2). The calculated VDEs for the global minimum of B_{23}^- are compared with those of the experiment in Table 1 and are plotted as vertical bars in Figure 2. The agreement between theory and experiment is excellent. Clearly the X band contains two detachment channels, corresponding to electron removal from the HOMO and HOMO−1. The relatively simple spectral pattern of B_{23}^- (Figure 2), compared with the broad spectrum of B_{22}^-, suggests that it comes only from one isomer, i.e., the global minimum of B_{23}^-, consistent with the fact that the heart-shaped structure is much more stable than any other structures. The very high electron binding energies of B_{23}^- also suggest that the heart-shaped structure is an exceptionally stable electronic system, which is borne out from the chemical bonding analyses, as discussed below.

6. STRUCTURES AND CHEMICAL BONDING

6.1. B_{22}^{2-}: An All-Boron Anthracene. The chemical bonding analysis of B_{22}^- was done on the basis of the canonical molecular orbitals (CMOs). The C_2 structure is not perfectly planar, and therefore, the division of the electron density into σ and π can be done only upon artificially flattening the structure to prevent mixing of σ and π orbitals. Since the out-of-plane distortion in the C_2 B_{22}^- is relatively small, the analyses using the perfectly planar system should capture the main features of the chemical bonding in the C_2 B_{22}^- species. Our analysis is actually based on the closed-shell planar B_{22}^{2-} species. We found that B_{22}^{2-} contains seven CMOs reminiscent of those in anthracene ($C_{14}H_{10}$), as shown in Figure 5. Therefore, the planar B_{22}^{2-} can be considered as an all-boron analogue of anthracene. An AdNDP analysis (not shown) reveals that the peripheral 14 boron atoms are bonded by 14 2c−2e bonds, whereas the bonding among the 8 interior atoms and between the interior and the peripheral ring is via delocalized σ and π bonds. The B_{22}^- cluster is thus one electron short of an all-boron analogue of anthracene, or it can be viewed as an all-boron analogue of the anthracene cation ($C_{14}H_{10}^+$).

dx.doi.org/10.1021/ja307605t | J. Am. Chem. Soc. 2012, 134, 18065−18073

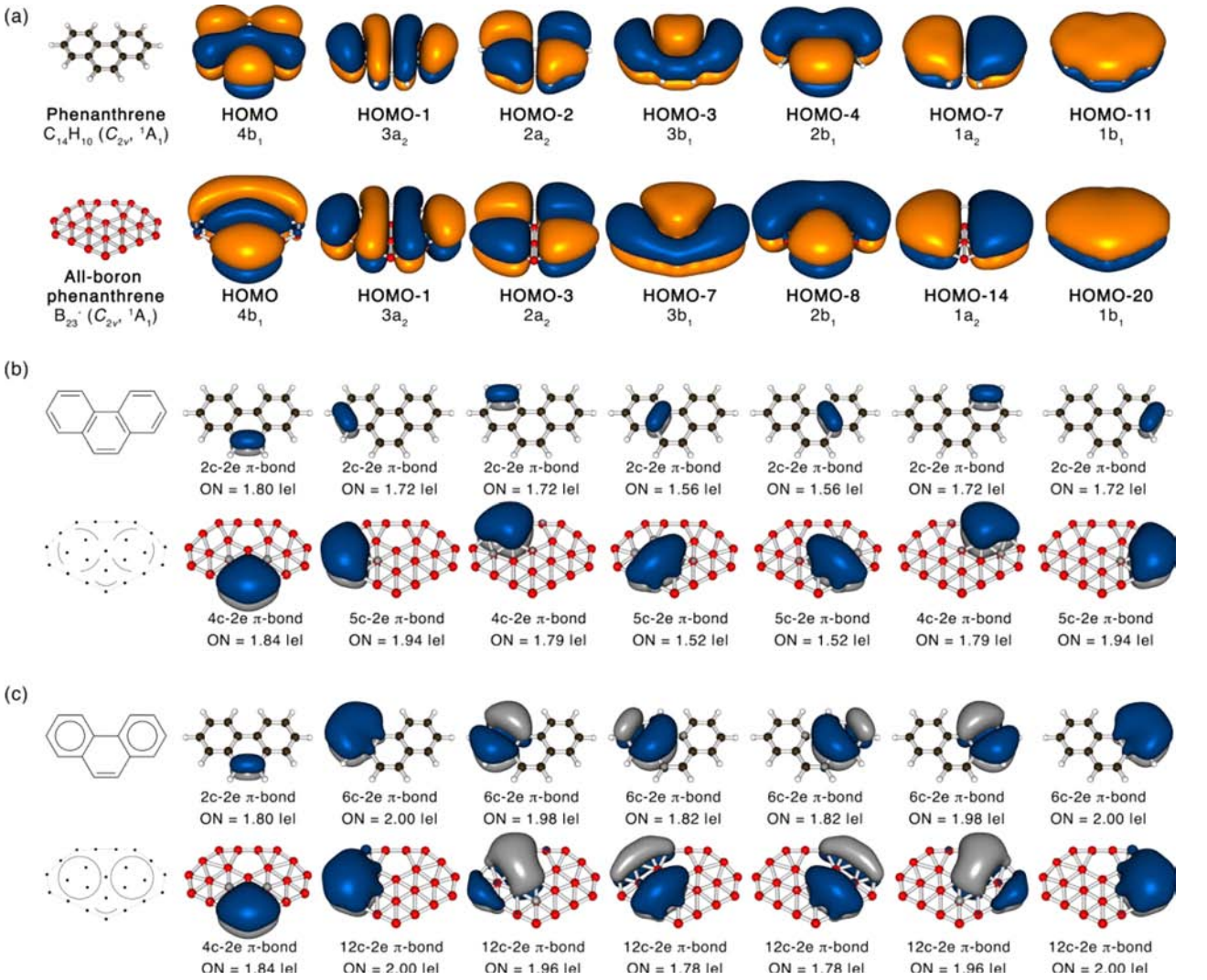

Figure 6. Elucidation of the analogy between the π bonding in B_{23}^- and phenanthrene. (a) Comparison of the π molecular orbitals, (b) comparison of the Kekule-type π-bonds obtained by the AdNDP method, (c) comparison of the Clar-type π-bonds obtained by the AdNDP method.

The C_2 structure of B_{22}^- has a regular, but buckled, triangular lattice. The buckling in B_{22}^- is entirely due to the geometrical constraint of the 14-atom periphery, which cannot host 8 interior atoms. All 2D boron clusters possess a periphery characterized by strong 2c−2e σ bonds, resulting in shorter B−B distances in the periphery than B−B distances in the interior, where only delocalized bonding exists (except B_{21}^-). A regular planar triangular boron lattice requires equal B−B distances throughout the 2D structure, which is incompatible with the strong peripheral bonding and weaker interior bonding. Therefore, either a 2D planar boron cluster buckles to give quasi-planar structures or holes will result in the interior of a perfectly planar boron cluster to release the geometrical strain caused by the strong peripheral B−B bonds. This is also why infinitely large planar boron sheets have to contain hexagonal holes, rather than a regular triangular lattice.[19] In the current case, even the doubly charged B_{22}^{2-} is not stable as a perfectly planar triangular lattice. Structural optimization shows that it is also slightly buckled similar to the C_2 B_{22}^- monoanion.

6.2. B_{23}^- (C_{2v}, $^1A_1$): An All-Boron Phenanthrene. We have performed a more thorough chemical bonding analysis of B_{23}^-, using both the CMOs and the AdNDP method, and discovered that the π bonding in B_{23}^- is almost identical to that in phenanthrene, as shown in Figure 6. First, we compared the π CMOs of B_{23}^- with those of phenanthrene in Figure 6a. The similarity between the π orbitals of the two molecules is extraordinary: they all have exactly the same irreducible representations and nodal structures. Such a high degree of semblance between the π bonding of a planar boron cluster and a hydrocarbon is unprecedented among all the planar boron clusters characterized so far. Hence, the B_{23}^- nanoheart can be considered as an all-boron analogue of phenanthrene, an isomer of anthracene ($C_{14}H_{10}$) also composed of three fused benzene rings.

The AdNDP method allows us to obtain alternative chemical bonding representations, which reinforce the remarkable analogy between the B_{23}^- nanoheart and phenanthrene. The AdNDP approach is based on the idea that the valence electron density can be partitioned into sets of two-electron objects, which can be either localized (1c−2e Lewis-type lone pairs or 2c−2e Lewis-type localized bonds) or delocalized (nc−2e bonds, $n > 2$). The partitioning of the electron density using the AdNDP method leads to a chemical-bonding picture consistent with the symmetry of the wave function and the molecule itself. If there is more than one way to partition the electron density using the AdNDP method, the model that produces higher

dx.doi.org/10.1021/ja307605t | J. Am. Chem. Soc. 2012, 134, 18065−18073

occupation numbers (ON) of bonds is believed to be more accurate.

The AdNDP analysis for phenanthrene (Figure S1 in SI) reveals 16 2c−2e C−C and 10 2c−2e C−H σ bonds. However, the π density in phenanthrene can be partitioned in two ways: (1) the Kekule representation with seven localized π bonds (Figure 6b and Figure S1 in SI); (2) the Clar representation with benzene-like delocalization of six π electrons over each of the outer benzene rings and one localized π bond in the central hexagon (Figure 6c and Figure S2 in SI). Comparison of the ONs of the AdNDP bonds suggests that the Clar representation of the chemical bonding is a more accurate model, in agreement with the chemical-bonding picture of phenanthrene proposed recently.[38b]

Partitioning the π electron density in B_{23}^-, similarly using AdNDP, we also obtain two representations of the π-bonding pattern: the Kekule type (Figure 6b) and the Clar type (Figure 6c), which are analogous to the corresponding set in phenanthrene. Again, the Clar representation has higher ONs and should be considered a more accurate representation of the delocalized π bonding in the B_{23}^- nanoheart. According to the AdNDP analyses, the σ electrons in B_{23}^- form 15 2c−2e peripheral B−B σ bonds and 13 delocalized σ bonds inside of the heart-shaped cluster, as shown in Figures S3 and S4. Therefore, both the delocalized π and σ electrons in B_{23}^- conform to the $4n + 2$ Hückel rule, rendering the nanoheart doubly aromatic. The pentagonal hole and the double aromaticity underlie the perfectly planar structure and high stability of the B_{23}^- nanoheart.

It is interesting to compare the electronic structures of the planar B_{23}^- with the predicted most stable form of a 2D boron sheet, i.e., the α-sheet.[19] The α-sheet contains regular hexagonal holes, in which the ratio of σ and π electrons is 3 to 1, identical to that in graphene. In B_{23}^-, the σ and π electron ratio is 4 to 1, whereas that in B_{22}^- is very close to 4 to 1. The lower π occupancy in the boron cluster is due to the fact that there is no hole in the B_{22}^- structure or only a pentagonal hole in the B_{23}^- nanoheart. It is expected that in larger planar boron clusters hexagonal holes may appear, which will increase the π occupancy because of reduced in-plane σ bonds. It would be interesting to see if such planar boron clusters exist and at what size. The existence of such planar clusters would confirm the viability of the predicted α-sheet.[19]

The analogy between the π bonding in B_{22}^-, B_{23}^-, and polycyclic aromatic hydrocarbons suggests that they may exhibit similar electronic properties in the bulk. Anthracene and phenanthrene are important organic molecular semiconductors. Both B_{22}^- and B_{23}^- have lateral dimensions over 1 nm. If these planar boron nanoclusters can be deposited on surfaces, their electrical properties can be potentially investigated by scanning tunneling microscopy. They are expected to display similar electrical properties. Neutral B_{22} is closed shell and should display semiconducting properties, whereas neutral B_{23} is open shell and should be a conductor.

7. CONCLUSIONS

We report a joint photoelectron spectroscopy and ab initio study of B_{22}^- and B_{23}^-, the largest boron cluster anions to be characterized heretofore. Two different global minimum search methods were used, and comparison between theory and experiment concluded that negatively charged boron clusters continue to be planar or quasi-planar up to 23 atoms. The global minimum of B_{22}^- is found to be quasi-planar with a slightly buckled triangular lattice consisting of 14 peripheral and 8 interior boron atoms. Chemical bonding analyses for a flattened B_{22}^{2-} reveal that its π-bonding pattern is similar to that in anthracene. Hence, the quasi-planar B_{22}^- cluster can be viewed as an all-boron analogue of an anthracene cation. The B_{23}^- cluster is found to possess a perfectly planar and heart-shaped structure consisting of a 15-atom periphery with 8 interior atoms and a pentagonal hole. The π bonding in B_{23}^- is found to be identical to that in phenanthrene. The B_{23}^- nanoheart is found to be particularly stable, derived from its perfectly planar structure and double aromaticity. The current study extends the family of all-boron analogues of aromatic hydrocarbons and demonstrates that boron clusters provide a fertile ground to discover interesting structures and bonding.

■ ASSOCIATED CONTENT

Supporting Information

Complete ref 37; AdNDP analyses of phenanthrene and B_{23}^- according to Kekule and Clar representations; theoretical VDEs of the low-lying isomers of B_{22}^- and B_{23}^-; Cartesian coordinates of the low-lying isomers of B_{22}^- and B_{23}^-. This material is available free of charge via the Internet at http://pubs.acs.org.

■ AUTHOR INFORMATION

Corresponding Author

A.I.Boldyrev@usu.edu (A.I.B.); Lai-Sheng_Wang@brown.edu (L.S.W.).

Author Contributions

[§]These authors contributed equally.

Notes

The authors declare no competing financial interest.

■ ACKNOWLEDGMENTS

This research was supported by the National Science Foundation (DMR-0904034 to L.S.W. and CHE-1057746 to A.I.B.). Computer time from the Center for High Performance Computing at Utah State University is gratefully acknowledged. The computational resource, the Uinta cluster supercomputer, was provided through the National Science Foundation under Grant CTS-0321170 with matching funds provided by Utah State University. This work used the Extreme Science and Engineering Discovery Environment (XSEDE), which is supported by National Science Foundation Grant Number OCI-1053575. This work was also partially supported by Brown University through the use of the facilities of its Center for Computation and Visualization.

■ REFERENCES

(1) (a) Vast, N.; Baronia, S.; Zerah, G.; Besson, J. M.; Polian, A.; Grimsditch, M.; Chervin, J. C. *Phys. Rev. Lett.* **1997**, *78*, 693−696. (b) Fujimori, M.; Nakata, T.; Nakayama, T.; Nishibori, E.; Kimura, K.; Takata, M.; Sakata, M. *Phys. Rev. Lett.* **1999**, *82*, 4452−44525.

(2) (a) Zhai, H. J.; Wang, L. S.; Alexandrova, A. N.; Boldyrev, A. I. *J. Chem. Phys.* **2002**, *117*, 7917−7924. (b) Alexandrova, A. N.; Boldyrev, A. I.; Zhai, H. J.; Wang, L. S.; Steiner, E.; Fowler, P. W. *J. Phys. Chem. A* **2003**, *107*, 1359−1369. (c) Alexandrova, A. N.; Boldyrev, A. I.; Zhai, H. J.; Wang, L. S. *J. Phys. Chem. A* **2004**, *108*, 3509−3517. (d) Zhai, H. J.; Wang, L. S.; Alexandrova, A. N.; Boldyrev, A. I.; Zakrzewski, V. G. *J. Phys. Chem. A* **2003**, *107*, 9319−9328. (e) Alexandrova, A. N.; Boldyrev, A. I.; Zhai, H. J.; Wang, L. S. *J. Chem. Phys.* **2005**, *122*, 054313.

(3) Zhai, H. J.; Alexandrova, A. N.; Birch, K. A.; Boldyrev, A. I.; Wang, L. S. *Angew. Chem., Int. Ed.* **2003**, *42*, 6004−6008. (b) Alexandrova, A. N.; Zhai, H. J.; Wang, L. S.; Boldyrev, A. I. *Inorg. Chem.* **2004**, *43*, 3552−3554.
(4) Zhai, H. J.; Kiran, B.; Li, J.; Wang, L. S. *Nature Mater.* **2003**, *2*, 827−833.
(5) Kiran, B.; Bulusu, S.; Zhai, H. J.; Yoo, S.; Zeng, X. C.; Wang, L. S. *Proc. Natl. Acad. Sci. U.S.A.* **2005**, *102*, 961−964.
(6) Alexandrova, A. N.; Boldyrev, A. I.; Zhai, H. J.; Wang, L. S. *Coord. Chem. Rev.* **2006**, *250*, 2811−2866.
(7) (a) Zhai, H. J.; Wang, L. S.; Zubarev, D. Y.; Boldyrev, A. I. *J. Phys. Chem. A.* **2006**, *110*, 1689−1693. (b) Wang, L. M.; Huang, W.; Averkiev, B. B.; Boldyrev, A. I.; Wang, L. S. *Angew. Chem., Int. Ed.* **2007**, *46*, 4550−4553. (c) Averkiev, B. B.; Zubarev, D. Y.; Wang, L. M.; Huang, W.; Wang, L. S.; Boldyrev, A. I. *J. Am. Chem. Soc.* **2008**, *130*, 9248−9250. (d) Averkiev, B. B.; Wang, L. M.; Huang, W.; Wang, L. S.; Boldyrev, A. I. *Phys. Chem. Chem. Phys.* **2009**, *11*, 9840−9849.
(8) Sergeeva, A. P.; Zubarev, D. Y.; Zhai, H. J.; Boldyrev, A. I.; Wang, L. S. *J. Am. Chem. Soc.* **2008**, *130*, 7244−7246.
(9) Pan, L. L.; Li, J.; Wang, L. S. *J. Chem. Phys.* **2008**, *129*, 024302.
(10) Huang, W.; Sergeeva, A. P.; Zhai, H. J.; Averkiev, B. B.; Wang, L. S.; Boldyrev, A. I. *Nature Chem.* **2010**, *2*, 202−206.
(11) (a) Wang, L. M.; Averkiev, B. B.; Ramilowski, J. A.; Huang, W.; Wang, L. S.; Boldyrev, A. I. *J. Am. Chem. Soc.* **2010**, *132*, 14104−14112. (b) Zhai, H. J.; Miao, C. Q.; Li, S. D.; Wang, L. S. *J. Phys. Chem. A* **2010**, *114*, 12155−12161. (c) Galeev, T. R.; Ivanov, A. S.; Romanescu, C.; Li, W. L.; Bozhenko, K. V.; Wang, L. S.; Boldyrev, A. I. *Phys. Chem. Chem. Phys.* **2011**, *13*, 8805−8810. (d) Romanescu, C.; Sergeeva, A. P.; Li, W. L.; Boldyrev, A. I.; Wang, L. S. *J. Am. Chem. Soc.* **2011**, *133*, 8646−8653.
(12) Sergeeva, A. P.; Averkiev, B. B.; Zhai, H. J.; Boldyrev, A. I.; Wang, L. S. *J. Chem. Phys.* **2011**, *134*, 224304.
(13) Piazza, Z. A.; Li, W. L.; Romanescu, C. R.; Sergeeva, A. P.; Wang, L. S.; Boldyrev, A. I. *J. Chem. Phys.* **2012**, *136*, 104310.
(14) Romanescu, C.; Harding, D. J.; Fielicke, A.; Wang, L. S. *J. Chem. Phys.* **2012**, *137*, 014317.
(15) Oger, E.; Crawford, N. R. M.; Kelting, R.; Weis, P.; Kappes, M. M.; Ahlrichs, R. *Angew. Chem., Int. Ed.* **2007**, *46*, 8503−8506.
(16) (a) Hanley, L.; Whitten, J. L.; Anderson, S. L. *J. Phys. Chem.* **1988**, *92*, 5803−5812. (b) Hintz, P. A.; Ruatta, S. A.; Anderson, S. L. *J. Chem. Phys.* **1990**, *92*, 292−303. (c) Ruatta, S. A.; Hintz, P. A.; Anderson, S. L. *J. Chem. Phys.* **1991**, *94*, 2833−2847. (d) Sowa-Resat, M. B.; Smolanoff, J.; Lapiki, A.; Anderson, S. L. *J. Chem. Phys.* **1997**, *106*, 9511−9522.
(17) (a) Kawai, R.; Weare, J. H. *J. Chem. Phys.* **1991**, *95*, 1151−1159. (b) Kawai, R.; Weare, J. H. *Chem. Phys. Lett.* **1992**, *191*, 311−314.
(18) (a) Bonacic-Koutecky, V.; Fantucci, P.; Koutecky, J. *Chem. Rev.* **1991**, *91*, 1035−1108. (b) Martin, J. M. L.; François, J. P.; Gijbels, R. *Chem. Phys. Lett.* **1992**, *189*, 529−536. (c) Kato, H.; Yamashita, K.; Morokuma, K. *Chem. Phys. Lett.* **1992**, *190*, 361−366. (d) Boustani, I. *Int. J. Quantum Chem.* **1994**, *52*, 1081−1111. (e) Boustani, I. *Chem. Phys. Lett.* **1995**, *233*, 273−278. (f) Boustani, I. *Chem. Phys. Lett.* **1995**, *240*, 135−140. (g) Ricca, A.; Bauschlicher, C. W. *Chem. Phys.* **1996**, *208*, 233−242. (h) Boustani, I. *Surf. Sci.* **1997**, *370*, 355−363. (i) Boustani, I. *Phys. Rev. B* **1997**, *55*, 16426−16438. (j) Niu, J.; Rao, B. K.; Jena, P. *J. Chem. Phys.* **1997**, *107*, 132−140. (k) Gu, F. L.; Yang, X.; Tang, A. C.; Jiao, H.; Schleyer, P. v. R. *J. Comput. Chem.* **1998**, *19*, 203−214.
(19) (a) Tang, H.; Ismail-Beigi, S. *Phys. Rev. Lett.* **2007**, *99*, 115501. (b) Yang, X.; Ding, Y.; Ni, J. *Phys. Rev. B* **2008**, *77*, 041402. (c) Tang, H.; Ismail-Beigi, S. *Phys. Rev. B* **2009**, *80*, 134113. (d) Galeev, T. R.; Chen, Q.; Guo, J. C.; Bai, H.; Miao, C. Q.; Lu, H. G.; Sergeeva, A. P.; Li, S. D.; Boldyrev, A. I. *Phys. Chem. Chem. Phys.* **2011**, *13*, 11575−11578.
(20) Fowler, P. W.; Gray, B. R. *Inorg. Chem.* **2007**, *46*, 2892−2897.
(21) (a) Fowler, J. E.; Ugalde, J. M. *J. Phys. Chem. A* **2000**, *104*, 397−403. (b) Aihara, J. *J. Phys. Chem. A* **2001**, *105*, 5486−5489. (c) Zubarev, D. Yu.; Boldyrev, A. I. *J. Comput. Chem.* **2007**, *28*, 251−268.
(22) (a) Romanescu, C.; Galeev, T. R.; Li, W. L.; Boldyrev, A. I.; Wang, L. S. *Angew. Chem., Int. Ed.* **2011**, *50*, 9334−9337. (b) Li, W. L.; Romanescu, C.; Galeev, T. R.; Piazza, Z. A.; Boldyrev, A. I.; Wang, L. S. *J. Am. Chem. Soc.* **2012**, *134*, 165−168. (c) Galeev, T. R.; Romanescu, C.; Li, W. L.; Wang, L. S.; Boldyrev, A. I. *Angew. Chem., Int. Ed.* **2012**, *51*, 2101−2105. (d) Romanescu, C.; Galeev, T. R.; Sergeeva, A. P.; Li, W. L.; Wang, L. S.; A. I. Boldyrev, A. I. *J. Organomet. Chem.* **2012**, DOI: 10.1016/j.jorganchem.2012.07.050.
(23) Jimenez-Halla, J. O. C.; Islas, R.; Heine, T.; Merino, G. *Angew. Chem., Int. Ed.* **2010**, *49*, 5668−5671.
(24) Martínez-Guajardo, G.; Sergeeva, A. P.; Boldyrev, A. I.; Heine, T.; Ugalde, J. M.; Merino, G. *Chem. Commun.* **2011**, *47*, 6242−6244.
(25) Zhang, J.; Sergeeva, A. P.; Sparta, M.; Alexandrova, A. N. *Angew. Chem., Int. Ed.* **2012**, *51*, 8512−8515.
(26) Popov, I. A.; Boldyrev, A. I. *J. Phys. Chem. C* **2012**, *116*, 3147−3152.
(27) (a) Kiran, B.; Kumar, G. G.; Nguyen, M. T.; Kandalam, A. K.; Jena, P. *Inorg. Chem.* **2009**, *48*, 9965−9967. (b) Truong, B. T.; Grant, D. J.; Nguyen, M. T.; Dixon, D. A. *J. Phys. Chem. A* **2010**, *114*, 994−1007. (c) Truong, B. T.; Nguyen, M. T.; Nguyen, M. T. *Chem. Phys. Lett.* **2012**, *530*, 71−76. (d) Truong, B. T.; Ceulemans, A.; Nguyen, M. T. *Chem.—Eur. J.* **2012**, *18*, 4510−4512. (e) Li, F.; Jin, P.; Jiang, D. E.; Wang, L.; Zhang, S. B.; Zhao, J.; Chen, Z. F. *J. Chem. Phys.* **2012**, *136*, 074302.
(28) Schönbom, S. E.; Goedecker, S.; Roy, S.; Oganov, A. R. *J. Chem. Phys.* **2009**, *130*, 144108.
(29) (a) Averkiev, B. B. Geometry and Electronic Structure of Doped Clusters via the Coalescence Kick Method. PhD Dissertation; Utah State University: Logan, UT, 2009. (b) Saunders, M. *J. Comput. Chem.* **2004**, *25*, 621−626. (c) Bera, P. P.; Sattlemeyer, K. W.; Saunders, M.; Schaefer, H. F.; Schleyer, P. v. R. *J. Phys. Chem. A* **2006**, *110*, 4287−4290.
(30) (a) Wang, L. S.; Cheng, H. S.; Fan, J. *J. Chem. Phys.* **1995**, *102*, 9480−9493. (b) Wang, L. S.; Wu, H. In *Advances in Metal and Semiconductor Clusters*; Duncan, M. A., Ed.; JAI Press: Greenwich, 1998; pp 299−343.
(31) (a) Huang, W.; Wang, L. S. *Phys. Rev. Lett.* **2009**, *102*, 153401. (b) Akola, J.; Manninen, M.; Hakkinen, H.; Landman, U.; Li, X.; Wang, L. S. *Phys. Rev. B* **1999**, *60*, R11297−R11300. (c) Wang, L. S.; Li, X. In *Proc. Int. Symp. Clusters Nanostructure Interfaces*; Jena, P.; Khanna, S. N.; Rao, B. K., Eds.; World Scientific: River Edge, NJ, 2000; pp 293−300.
(32) (a) Bilodeau, R. C.; Haugen, H. K. *Phys. Rev. A* **2001**, *64*, 024501. (b) Feigerle, C. S.; Corderman, R. R.; Bobashev, S. V.; Lineberger, W. C. *J. Chem. Phys.* **1981**, *74*, 1580−1582.
(33) (a) Perdew, J. P.; Burke, K.; Ernzerhof, M. *Phys. Rev. Lett.* **1996**, *77*, 3865−3868. (b) Perdew, J. P.; Burke, K.; Ernzerhof, M. *Phys. Rev. Lett.* **1997**, *78*, 1396−13969. (c) Adamo, C.; Barone, V. *J. Chem. Phys.* **1999**, *110*, 6158−6170.
(34) Binkley, J. S.; Pople, J. A.; Hehre, W. J. *J. Am. Chem. Soc.* **1980**, *102*, 939−947.
(35) (a) Gordon, M. S.; Binkley, J. S.; Pople, J. A.; Pietro, W. J.; Hehre, W. J. *J. Am. Chem. Soc.* **1982**, *104*, 2797−2803. (b) Pietro, W. J.; Francl, M. M.; Hehre, W. J.; Defrees, D. J.; Pople, J. A.; Binkley, J. S. *J. Am. Chem. Soc.* **1982**, *104*, 5039−5048. (c) Clark, T.; Chandrasekhar, J.; Spitznagel, G. W.; Schleyer, P. v. R. *J. Comput. Chem.* **1983**, *4*, 294−301.
(36) (a) Cizek. *J. Adv. Chem. Phys.* **1969**, *14*, 35−45. (b) Purvis, G. D.; Bartlett, R. J. *J. Chem. Phys.* **1982**, *76*, 1910−1918. (c) Raghavachari, K.; Trucks, G. W.; Pople, J. A.; Head-Gordon, M. *Chem. Phys. Lett.* **1989**, *157*, 479−483.
(37) Frisch, M. J.; et al. *Gaussian 09*, Revision B.01; Gaussian, Inc.: Wallingford, CT, 2010.
(38) (a) Zubarev, D. Y.; Boldyrev, A. I. *Phys. Chem. Chem. Phys.* **2008**, *10*, 5207−5217. (b) Zubarev, D. Y.; Boldyrev, A. I. *J. Org. Chem.* **2008**, *73*, 9251−9258. (c) Zubarev, D. Y.; Boldyrev, A. I. *J. Phys. Chem. A* **2009**, *113*, 866−868.
(39) Sergeeva, A. P.; Boldyrev, A. I. *Comments Inorg. Chem.* **2010**, *31*, 2−12.

(40) Varetto, U. *MOLEKEL*, 5.4.0.8; Swiss National Supercomputing Centre: Manno, Switzerland, 2009.
(41) Norm values indicate multiconfigurational contributions to the CCSD(T) wave functions. A norm value of larger than 1.5 is considered high in CCSD(T) calculations. Isomers I–IV of B_{22}^- all have norm values near or above 1.5.